Intrafacet migration effects in InGaN/GaN structures grown on triangular GaN ridges studied by submicron beam x-ray diffraction

P. L. Bonanno,[1,a)] S. M. O'Malley,[1] A. A. Sirenko,[1] A. Kazimirov,[2] Z.-H. Cai,[3] T. Wunderer,[4] P. Brückner,[4] and F. Scholz[4]
[1]*Department of Physics, New Jersey Institute of Technology, Newark, New Jersey 07102, USA*
[2]*Cornell High Energy Synchrotron Source (CHESS), Cornell University, Ithaca, New York 14853, USA*
[3]*Advanced Photon Source, 9700 S. Cass Avenue, Argonne, Illinois 60439, USA*
[4]*Institute of Optoelectronics, University of Ulm, 89081 Ulm, Germany*

(Received 19 January 2008; accepted 3 March 2008; published online 26 March 2008)

Synchrotron radiation has been utilized for x-ray diffraction and reciprocal space mapping of InGaN/GaN multiple-quantum-well (MQW) structures grown on the sidewalls of 10-μm-wide triangular GaN ridges with $\{1-1.1\}$ facets. Samples were produced by lateral overgrowth through a patterned dielectric mask by using metal-organic vapor-phase epitaxy. Global MQW strain, period, and the tilt of the (00.1) crystallographic planes have been measured across the sidewall facets using a 240 nm x-ray beam. Results of this study are interpreted in terms of suppressed intrafacet migration of In and Ga precursors during the MQW growth. © *2008 American Institute of Physics*. [DOI: 10.1063/1.2901142]

The optical efficiency of GaN-based light-emitting devices grown on the commonly used *c*-plane of GaN (00.1) is hindered by large piezoelectric fields within the active region.[1] One way to alleviate this problem is to grow devices on the semipolar planes of GaN ridge structures.[2] Ridge formation is generated when GaN is grown between dielectric masks patterned on the wafer surface in a process known as selective-area-growth (SAG).[3] Semipolar sidewall facets are formed during metal-organic vapor phase epitaxy (MOVPE) of GaN. The overgrowth wing region exhibits additional properties compared to planar GaN-based structures. One of them is a few degree tilt of the (00.1) planes.[4] Further progress in this technology requires development of suitable characterization methods such as microbeam x-ray diffraction (XRD),[5–7] spatially resolved XRD imaging,[8] and cathodoluminescence microscopy.[9] In this letter, we apply nondestructive synchrotron-based submicron beam XRD with a spatial resolution of 240 nm along with reciprocal-space-mapping (RSM) to determine the period, strain, and (00.1) planar tilt in SAG ridges with InGaN/GaN multiple-quantum-well (MQW) structures. Trends in strain and MQW period are interpreted within the framework of the intrafacet migration of Ga and In precursors.

Samples were grown by low-pressure MOVPE in a single-wafer Aixtron system with a horizontal reactor design. A GaN buffer layer was grown epitaxially on *c*-plane sapphire substrates. A 200 nm thick SiO_2 oxide mask was deposited on the GaN buffer layer by plasma enhanced chemical vapor deposition and patterned by optical lithography and reactive ion etching. The sample consisted of an array of 20 μm wide oxide stripes oriented along the $\langle 11.0 \rangle$ crystallographic direction of GaN and separated by 3 μm wide open regions exposing the GaN buffer layer. *n*-doped GaN ridges were subsequently grown inside the unmasked regions with reactor conditions optimized to produce ridges with triangular cross sections terminated by $\{1-1.1\}$ sidewall facets. The typical base size of the ridges was ~10 μm as resulted from significant overgrowth of GaN over the mask. A MQW structure consisting of three InGaN quantum wells separated by GaN barriers was then grown on the GaN ridge at reduced growth temperature that increased indium incorporation. Lastly, the device structure was finished with a *p*-doped Mg:GaN capping layer grown with a target thickness of ~0.2 μm. Sample growth details and results of scanning electron microscopy (SEM), transmission electron microscopy (TEM), and optical characterization are described in detail in Ref. 2.

XRD characterization of the InGaN/GaN MQW structure was carried out using synchrotron radiation with an x-ray energy of 10.5 keV at the 2-ID-D micro-diffraction beamline at APS (see Fig. 1). A zone plate was utilized to focus an x-ray beam to a semicircular spot with a diameter of ~240 nm. The approximately 160 arc sec divergence of the beam has limited the angular resolution of our measurements.[7] Previous measurements on these samples using a high-angular resolution macro-beam setup at Cornell High Energy Synchrotron Source show that broadening of rocking curves due to mosaic spread is in the range of 120–150 arc sec. Samples were mounted on an *XYZ* stage, which enabled cross sectional XRD measurements. The position of the x-ray beam on the sample surface was controlled with 50 nm precision by simultaneous monitoring of the Ga-*K* fluorescence from the ridges. Diffracted intensity was collected by a large-area charge coupled device (CCD) detector positioned on the 2θ arm of a Newport diffractometer. The interpixel distance and, hence, the resolution along both the 2θ and χ directions corresponded to ~16 arc sec. In the

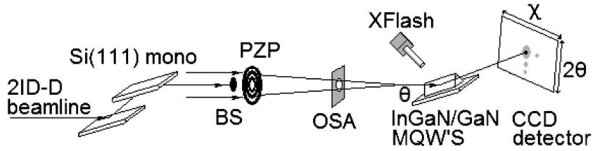

FIG. 1. Experimental setup. Si(111) mono—silicon monochromator; BS—gold beam stop; PZP—phase zone plate; OSA—order sorting aperture; XFlash—fluorescence detector.

a)Electronic mail: plb2@njit.edu.

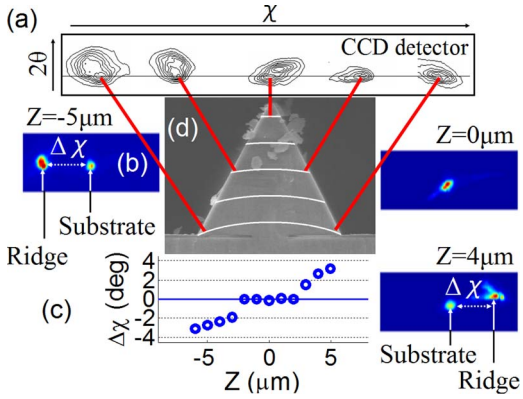

FIG. 2. (Color online) (a) A qualitative illustration of the tilt of the {00.1} planes observed as an azimuthal shift $\Delta\chi$ of the Bragg (00.2) reflection on the CCD detector. (b) An example CCD image shows the definition of $\Delta\chi$ as the difference in χ between (00.2) GaN reflection from the ridge and that from the substrate. (c) Azimuthal shift $\Delta\chi$ as a function of the position Z from the apex of the ridge. (d) SEM image of a single GaN ridge with InGaN/GaN MQWs grown at the sidewalls (not resolved) with the tilt of horizontal {00.1} planes shown schematically with white curves.

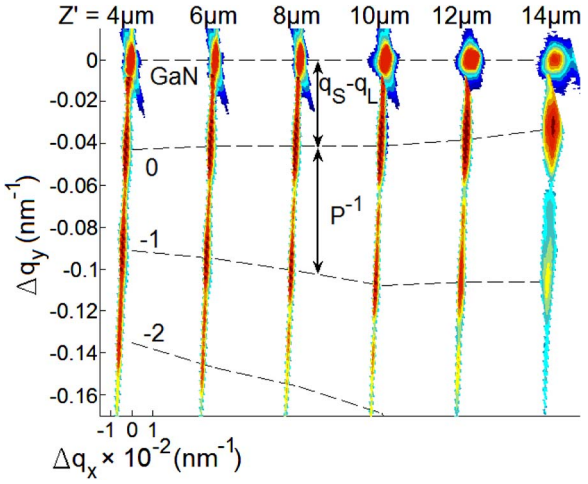

FIG. 3. (Color online) The (1−1.1) reciprocal-space maps measured for selected positions on the ridge sidewall. The distance Z' from the apex of the ridge is shown in microns on the top of the plot. The MQW satellite peaks are marked according to their order. The origin $\Delta q_x=\Delta q_y=0$ corresponds to the (1−1.1) reflection from the substrate. The FWHM of the satellites in q_x direction is comparable to the beam divergence (~160 arc sec) of our experimental setup. The larger widths of the GaN substrate peaks are due to color scale saturation.

following we will present results of the diffraction measurements for (00.2) and (1−1.1) symmetric reflections measured with ridges oriented along the diffraction plane.

Figure 2 shows the results of the tilt study for the (00.1) crystallographic planes. The x-ray beam was positioned at different locations across the ridge, and for each of these locations, CCD images of diffraction intensity were taken at Bragg conditions ($\chi_B=0°$, $\theta_B=13.18°$) for the (00.2) reflection of the GaN substrate with the diffraction plane oriented perpendicular to the substrate surface. Figure 2(a) qualitatively shows the way in which the tilt of the (00.1) planes affect the χ position of the diffracted signal on the CCD detector. Figure 2(b) shows how the tilt $\Delta\chi_B$ is calculated from raw CDD data. Figure 2(c) shows the azimuthal shift $\Delta\chi_B$ of the Bragg reflection versus position of the x-ray beam across the ridge. The tilt increases as the beam moves away from the center of the ridge, becoming distinguishable from the central signal originating from the GaN substrate at ~3 μm from the ridge center, and quasilinearly increasing at a rate of ~0.6°/μm away from the apex, eventually reaching more than 3° by the edges of the ridge wings.

The (1−1.1) diffraction experiment was performed at $\chi_B=61.9°$ and $\theta_B=14.03°$ so that the ridge sidewalls were perpendicular to the diffraction plane. In this geometry, the periodicity and global strain of the MQW structure was measured by collecting the CCD images at different θ angles around the GaN (1−1.1) reflection. We used a set of 2θ projections calculated from CCD images measured over a narrow range ($\Delta\chi\approx0.2°$) at regular intervals of θ. A RSM was constructed for each spatial position across the ridge by using standard transformations between the θ and 2θ angles and reciprocal space coordinates q_x and q_y (see, e.g., Ref. 10), where q_x is along ⟨11.0⟩ and q_y is perpendicular to the sidewall (1−1.1) surface. RSMs from selected positions on the ridge sidewalls are shown in Fig. 3.

Figure 4 depicts the MQW period versus position along the sidewall. The MQW period was determined by the q_y separation between adjacent satellite peaks L_i and L_j: $P=(q_y^{L_i}-q_y^{L_j})^{-1}$. The MQW period is 22.5 nm at the apex of the ridge. It decreases quasi-linearly by 0.9 nm/μm along the sidewall reaching a minimum value of 11.6 nm at the base.

The strong variation of the MQW period across the ridge sidewall can only be explained by combining a vapor-phase diffusion model for selectively grown planar structures with surface migration effects of the group-III species. The MQW period P in Fig. 4 indicates that during the MQW growth, which occurs at reduced growth temperature, the intrafacet migration rate for precursors is less than that during the growth of the GaN ridge below. The apex of the ridge is closer to the stagnant layer of precursors in the gas phase. In addition, it can be slightly cooler than the base. Taking into account a relatively short vapor-phase diffusion length for both the In and Ga precursors (for example, $D/k\approx11$ μm for Ga),[11] we can assume that the gas-phase concentration of precursors around the ridge apex is higher than that for the

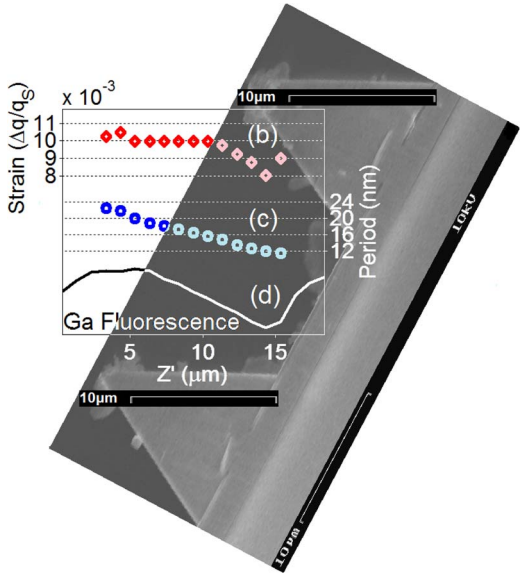

FIG. 4. (Color online) (a) SEM image of the ridge structure. The MQW global strain [(b) red diamonds], the period of the MQW [(c) blue circles], and the Ga fluorescence [(d) solid line] profiles are shown as functions of the distance Z' from the apex of the ridge.

ridge base. The vapor would then react with the GaN ridge near the apex, thereby promoting the higher growth rate. The reduced growth temperature (~800 °C) for the MWQ structure precludes redistribution of precursors across the sidewall facet effectively suppressing the intrafacet migration. Note that this scenario is different from the regime of GaN triangular ridge formation at elevated growth temperature (~1000 °C), where preservation of the $\{1-1.1\}$ sidewalls corresponds to a fairly constant growth rate across the ridge sidewall and, hence, a much faster rate of the interfacet surface migration of Ga precursors. Additionally, the D/k is certainly larger at 1000 °C than at 800 °C, i.e., the precursor molecules can diffuse to the bottom of the ridges more efficiently. For optoelectronic devices based on our structures, strong variation of the MQW period can result to broadband emission from the sidewall-grown structures, which is sometimes regarded as desirable for design of a white light source.[12]

Figure 4 presents the global MQW strain S^{MQW} for various position along the ridge sidewall: $S^{\mathrm{MQW}}=\Delta q/q_S$, where $q_S=4.108\ \mathrm{nm}^{-1}$ for $(1-1.1)$ reflection and Δq is the relative positions of the zeroth order MQW satellite peak (q_L) and the GaN substrate peak (q_S) along the q_y direction in the RSM, as shown in Fig. 3. Near the apex of the ridge, the global strain is approximately constant: $S^{\mathrm{MQW}}\approx 0.010$. By 8 μm from the apex (4 μm from the bottom), the strain begins to decrease at a rate of about $0.0005/\mu$m down the sidewall. Note that the strongest change of S^{MQW} occurs at the base, which hangs over the oxide mask. The observed trend for strain can be interpreted as an effect related to the emerging tilt of the (00.1) planes towards the substrate for the same part of the ridge.

The MQW strain values could help to estimate the indium composition x in the $\mathrm{In}_x\mathrm{Ga}_{x-1}\mathrm{N}$ quantum wells assuming that the well/barrier ratio is known from the growth time or TEM images. However, an assumption about relaxation should be made or several reflections should be analyzed to determine a and c parameters for the MQW layers. Still, conversion between a, c, and x in the $\mathrm{In}_x\mathrm{Ga}_{x-1}\mathrm{N}$ quantum wells is not trivial for the case of the triangular ridge geometry with stress-free $\{1-1.1\}$ sidewalls. For example, the conventional approach developed by Schuster *et al.*,[13] which utilizes Poisson's ratio for the c-plane oriented pseudomorphic layers, needs modification for the ridge structure geometry. Assuming complete strain relaxation and taking the barrier-to-well ratio $B/W\approx 2.2$ as approximated from the corresponding growth times, we estimate $x\approx 0.3$ for the $\mathrm{In}_x\mathrm{Ga}_{x-1}\mathrm{N}$ quantum wells at the apex and $x\approx 0.24$ at the base of the ridge. The latter is probably more accurate since the wings of the ridges should experience a higher degree of strain relaxation compared to the apex. Note that the estimated indium composition is quite high compared to the typical numbers of about 10%–15% for incorporation of indium in the $\mathrm{In}_x\mathrm{Ga}_{x-1}\mathrm{N}$ layers grown on planar $(00\bar{1})$ substrates. Systematic studies, which will include multiple XRD reflections, TEM analysis of the well/barrier ratio, and stress modeling, will be required to confirm the possibility of high indium incorporation in triangular ridges with $\{1-1.1\}$ oriented sidewalls.

We developed a nondestructive approach to combine RSMs and cross-sectional analytical studies for GaN-based ridge structures. A strong variation of the MQW period in InGaN/GaN structures was measured across the ridges. The growth rate of the MQW structure is two times higher at the top of the ridge compared to that at the base. This effect can be explained by suppression of the intrafacet migration for both Ga and In precursors compared to that for GaN ridge growth. Understanding of the growth rate and In composition variation on the submicron scale is important for growing MQW structures with strongly varying periods for the manufacturing of the broadband light-emitting devices.

Use of the Advanced Photon Source was supported by the U.S. Department of Energy, Office of Science, Office of Basic Energy Sciences, under Contract No. W-31-109-ENG-38. The Cornell High Energy Synchrotron Source was supported by the National Science Foundation and the National Institutes of Health/National Institute of General Medical Sciences under Award DMR-0225180. Parts of this work have been supported by the Deutsche Forschungsgemeinschaft.

[1] F. Bernardini, V. Fiorentini, and D. Vanderbilt, Phys. Rev. B **56**, R10024 (1997).
[2] T. Wunderer, P. Brückner, B. Neubert, F. Scholz, M. Feneberg, F. Lipski, M. Schirra, and K. Thonke, Appl. Phys. Lett. **89**, 041121 (2006).
[3] T. Takeuchi, H. Amano, and I. Akasaki, Jpn. J. Appl. Phys., Part 1 **39**, 413 (2000).
[4] P. Fini, H. Marchand, J. P. Ibbetson, S. P. DenBaars, U. K. Mishra, and J. S. Speck, J. Cryst. Growth **209**, 581 (2000).
[5] A. A. Sirenko, A. Kazimirov, S. Cornaby, D. H. Bilberback, B. Neubert, P. Brückner, F. Scholz, V. Shneidman, and A. Ougazzaden, Appl. Phys. Lett. **89**, 181926 (2006).
[6] A. A. Sirenko, A. Kazimirov, A. Ougazzaden, S. M. O'Malley, D. H. Bilderback, Z.-H. Cai, B. Lai, R. Huang, V. Gupta, M. Chien, and S. N. G. Chu, Appl. Phys. Lett. **88**, 081111 (2006).
[7] A. Kazimirov, A. A. Sirenko, D. H. Bilderback, Z.-H. Cai, B. Lai, R. Huang, and A. Ougazzaden, J. Phys. D **39**, 1422 (2006).
[8] D. Lubbert, T. Baumbach, P. Mikulik, P. Pernot, L. Helfen, R. Kohler, T. Katona, S. Keller, and S. P. DenBaars, J. Phys. D **38**, A50 (2005).
[9] Q. K. K. Liu, A. Hoffmann, H. Siegle, A. Kaschner, C. Thomsen, J. Christen, and F. Bertram, Appl. Phys. Lett. **74**, 3122 (1999).
[10] D. K. Bower and B. K. Tanner, *High Resolution X-ray Diffractomerty and Topography* (Taylor & Francis, London, 1998).
[11] M. E. Coltrin, C. C. Willan, M. E. Bartram, J. Han, N. Missert, M. H. Crawford, and A. G. Baca, MRS Internet J. Nitride Semicond. Res. **4S1**, G6.9 (1999).
[12] S. Srinivasan, M. Stevens, F. A. Ponce, and T. Mukai, Appl. Phys. Lett. **87**, 131911 (2005).
[13] M. Schuster, P. O. Gervais, B. Jobst, W. Hosler, R. Averbeck, H. Riechert, A. Iberl, and R. Stommer, J. Phys. D **32**, A56 (1999).